Polymer 335 (2025) 128771

Contents lists available at ScienceDirect

Polymer

journal homepage: www.elsevier.com/locate/polymer

A Graph Neural Network based deep learning framework for predicting the thermomechanical behavior of thermoset shape memory polymers☆

Khan Raqib Mahmud [a], Lingxiao Wang [b],*, Jinyuan Chen [b], Sunzid Hassan [a]

[a] Department of Computer Science, Louisiana Tech University, Ruston, 71272, LA, USA
[b] Department of Electrical Engineering, Louisiana Tech University, Ruston, 71272, LA, USA

ARTICLE INFO

Keywords:
Shape memory polymer
Epoxy–hardener compositions
Graph representations of polymers
Graph Neural Networks
Transformer model

ABSTRACT

Recent progress in machine learning (ML) and molecular simulations has made it possible to rapidly explore new formulations of Diamine-Hardened Epoxy-Based Thermoset Shape Memory Polymers (SMPs). However, accurate thermomechanical modeling, which is crucial for guiding the design of these advanced materials, still heavily relies on extensive experiments and simulations that are both time-consuming and costly. In this study, we propose a deep learning (DL) framework that integrates Graph Neural Networks (GNNs) and Time Series Transformers to accurately predict moving-averaged recovery stress in diamine-hardened epoxy-based thermoset SMPs. Specifically, a Graph Transformer is employed to encode atomic and bonding information derived from molecular SMILES (Simplified Molecular Input Line Entry System) representations into graph embeddings, which are dynamically updated and combined with sequential experimental data via a Time Series Transformer. Our model was trained end-to-end on molecular dynamics simulation data and validated across multiple epoxy–hardener formulations. The proposed approach consistently outperformed traditional deep learning models and achieved superior predictive accuracy, with a Root Mean Squared Error (RMSE) as low as 0.1895 and a Pearson Correlation Coefficient (PCC) of up to 1.000 on unseen datasets. These results highlight the significant potential of our framework to reduce dependency on extensive laboratory trials, and provide a robust, efficient, and scalable solution for rapid exploration and optimization of next-generation epoxy-based thermoset SMPs.

1. Introduction

Shape memory polymers (SMPs) are smart materials known for their unique ability to return to their original shapes after plastic deformation when triggered by external stimuli such as heat, light, electric currents, or changes in pH, electric, or magnetic fields [1,2]. This distinctive shape-memory effect arises from cross-linked polymer networks, which store elastic energy during deformation and release it upon stimulation to recover the original shape. Due to their responsiveness to multiple stimuli, SMPs are increasingly utilized in advanced fields such as biomedical applications, aerospace engineering, structural composites, and smart textiles [3–5].

Although SMPs offer significant potential, further developments are required to improve their properties and expand their application scope. Designing and validating new SMP formulations typically involve synthesizing novel polymers through a bottom-up approach, followed by extensive experimental testing to confirm desired characteristics. This conventional process requires considerable time, specialized expertise, and significant resources, thus it is inefficient and expensive for rapid material development [6].

To address this, our objective is to develop a deep learning framework that can accurately predict the moving-averaged recovery stress, a key thermomechanical property, of SMPs based on their molecular structure and experimental conditions. The motivation is to smooth out the rapid and noisy fluctuations inherent in the raw stress data by using a moving-averaged recovery stress. Our goal is not to reproduce every detail of, molecular dynamic (MD) simulations or experiments, but rather to accelerate polymer discovery by rapidly predicting structure-property trends across numerous formulations.

Accurate characterization of thermomechanical properties, particularly recoverable stress, is essential for guiding the design of SMPs, as it measures the polymer's capability to regain its original shape

---

☆ This work is supported by NSF EPSCoR LAMDA Seed Funding Track 1B with the contract number NSF(2024)-LAMDATr1B-22.

* Corresponding author.
E-mail address: lwang@latech.edu (L. Wang).

https://doi.org/10.1016/j.polymer.2025.128771
Received 13 May 2025; Received in revised form 1 July 2025; Accepted 3 July 2025

under external load following deformation. Thermomechanical analysis (TMA) is commonly employed to characterize these properties. TMA continuously records stress and strain responses while carefully varying temperature and external load, and provides insights into real-world behavior. Although TMA provides precise characterization, the necessity of performing repeated experiments for each unique SMP formulation introduces significant challenges. This iterative process demands considerable time, specialized resources, and high costs, thereby severely constraining the efficiency and speed of developing novel SMP materials.

Thermoset SMPs, in particular, are notable due to their permanent chemical cross-links that create rigid and stable polymer networks capable of robust shape recovery through internal stress rearrangement. The thermomechanical performance of thermoset SMPs, particularly their recovery stress, significantly depends on chemical composition, molecular weight, and cross-link density. Thermoset SMPs, specifically those that combine high recovery stress with moderate glass transition temperatures, are particularly valued in additive manufacturing (AM), which significantly broadens their potential applications to deployable structures, robotics, and self-healing materials [6–9].

Specifically, diamine-hardened epoxy-based thermoset SMPs derived from diglycidyl ether epoxy resins (e.g., Diglycidyl Ether of Bisphenol A, DGEBA) have received significant attention due to their exceptional mechanical properties, chemical resistance, and tunable shape-memory characteristics [6–9]. Adjusting epoxy–hardener combinations enables precise control over critical properties, such as mechanical strength, curing behavior, thermal stability, and shape recovery. Despite these promising attributes, the inherent brittleness of these epoxy-based SMPs poses a significant challenge, as high stress conditions can initiate cracks that propagate through their densely cross-linked networks and eventually causes material failure [10]. Experimentally exploring numerous epoxy–hardener combinations using traditional methods thus remains impractical and economically restrictive [11].

To overcome limitations associated with experimental approaches and the scarcity of comprehensive thermomechanical data, MD simulations offer an alternative for systematic data generation. Recent studies have effectively employed MD simulations to investigate cross-link behavior, thermomechanical cycles, and moving-averaged recovery stress correlations in epoxy–hardener SMP systems. For instance, MD simulations have revealed significant correlations between molecular modifications, such as variations in backbone length and side-chain structures, and moving-averaged recovery stress. These findings indicate that mechanical performance strongly depends on molecular-scale design choices.

Traditional thermomechanical modeling methods, including constitutive models e.g., Maxwell–Weichert [12] or Vogel–Fulcher–Tammann frameworks [13], typically depend heavily on experimental data for parameter fitting. This heavy reliance limits their generalizability across diverse polymer formulations. Similarly, micromechanics-based and finite element analysis (FEA) models, despite their effectiveness, have inherent constraints from assumptions and predefined parameters, which limit their adaptability for novel materials and dynamic conditions [8,9,14].

Recent advances in machine learning (ML), particularly deep learning (DL), have emerged as promising alternatives in materials science due to their computational efficiency and rapid predictive capabilities compared to traditional simulation techniques like MD and density functional theory (DFT) [15,16]. ML methods have demonstrated significant success across various material classes, optimizing properties such as mechanical strength in metal alloys [17], thermal conductivity in polymers [18], dielectric constants [19], and precisely targeted glass transition temperatures [20–23]. Additionally, ML-based constitutive modeling has shown substantial potential to capture complex mechanical behaviors of engineering materials, including solids and liquids, by employing supervised learning alongside physically informed constraints [24–27].

Combining ML with MD simulations has become an efficient pathway to expedite material discovery [6,28]. While MD simulations systematically investigate cross-linking behavior, thermomechanical cycles, and recovery stress, ML techniques leverage these simulation-generated or experimental datasets to predict optimal polymer formulations, significantly reducing the need to synthesize and experimentally validate every candidate. Molecular fingerprinting is a prominent approach in this context, translating each epoxy–hardener combination into atomistic descriptors, such as bond angles, ring structures, or partial charges. ML algorithms utilize these descriptors to correlate structural features with mechanical or shape-memory performance. However, despite a general theoretical understanding of how polymer structure influences their properties, accurately capturing and predicting the detailed molecular and topological structures remains challenging due to the complexity of computational modeling and the extensive time required for experimental validation.

Despite recent developments, accurately modeling the complex thermomechanical behavior of SMPs remains challenging. Current DL and ML approaches predominantly focus on temporal features alone and often overlook essential structural information derived from molecular configurations. Furthermore, gathering the substantial amount of experimental data required for ML training is costly and time-consuming due to the vast chemical space of potential epoxy–hardener formulations [11]. This limitation restricts predictive accuracy and generalization capabilities across diverse polymer systems. Consequently, there is a critical need for methods that effectively integrate structural characteristics with temporal data to enhance the precision and robustness of predictions.

To address this gap, we introduce a novel DL framework that integrates structural information extracted from molecular SMILES (Simplified Molecular Input Line Entry System) representations with temporal experimental data (temperature, time, and length) to accurately predict moving-averaged recovery stress, a critical thermomechanical property, in diamine-hardened epoxy-based thermoset SMPs. Our aim is to develop a DL framework for moving-averaged recovery stress prediction based on molecular and temporal features, which can accelerate the design of new SMP formulations. Specifically, our method employs a Graph Neural Network (GNN) to encode atomic and bonding characteristics of epoxy–hardener compositions into detailed graph embeddings. These embeddings, dynamically updated with sequential experimental data, are processed through a Time Series Transformer to predict moving-averaged stress behavior with high accuracy, as illustrated in Fig. 1. By structuring the input data into sliding windows of n consecutive time steps, our model predicts the moving-averaged stress at the final step of each window. This approach captures both structural and temporal dependencies within an end-to-end training framework and significantly enhances predictive performance and generalization across different polymer formulations.

The key contributions of this work can be listed as follows:

- We introduce a method to represent the SMILES strings of epoxy resins and hardeners into detailed graph representations, that encode the atom and bond features of the molecules.
- We develop graph transformer, a GNN based model, to capture the structural information and generate the graph embedding from the molecular graphs of epoxy–hardener.
- We propose a DL framework that integrates the Graph Transformer with a Time Series Transformer to predict the moving-averaged recovery stress of epoxy-hardener compositions and train the model in an end to end manner, to preserve the structural information as well as the temporal dependencies.

2. Methodology

2.1. Data collection and overview

The dataset used in this study is obtained from previously published MD simulations of amine-hardened epoxy-based thermoset SMPs [31,

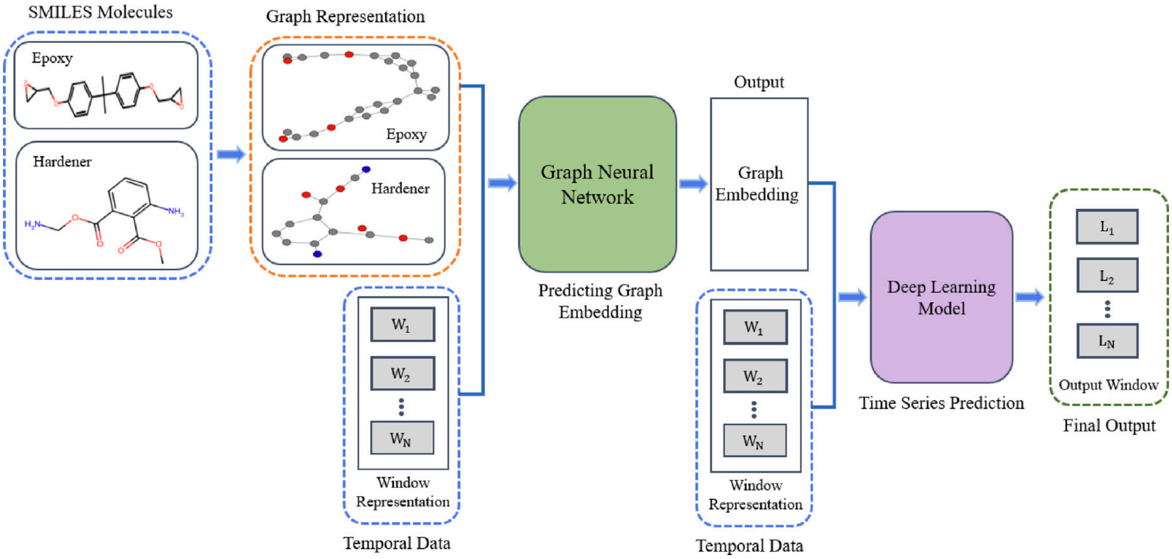

Fig. 1. An overview of the proposed methodology for predicting moving-averaged recovery stress of the composition of epoxy resins and hardener. The method generates graph representations from SMILES strings of the materials and takes them as input into the Graph Transformer model [29] that gives the graph embedding. This graph embedding combined with the temporal data pass through the Time Series Transformer [30] to predict the final output.

Table 1
Summary of temporal features for each epoxy–hardener SMP formulation.

Feature	Description
Time	Discrete time steps at which the polymer's response is recorded.
Temperature	The heating and cooling process that controls polymer softening and hardening for shape recovery.
Length	Macroscopic sample dimension along the loading axis, changes with time and temperature.
Moving-averaged stress	A smoothed measure of recovery stress, quantifying the material's ability to regain its shape after deformation.

Table 2
Epoxy resins used in this study.

Epoxy	Compound name	Description
DGEBA	Diglycidyl ether of Bisphenol A	Widely used commercial epoxy known for high recovery stress and mechanical strength.
DGEBF	Diglycidyl ether of Bisphenol F	Bio-based epoxy with furan rings, offering enhanced thermomechanical properties.
autoEpoxy	Computationally designed epoxies	A set of algorithmically generated epoxies comprising several variants, optimized for molecular rigidity, thermal stability, and improved recovery stress.

32]. These simulations capture the complete thermomechanical cycle of each epoxy–hardener formulation, including loading, relaxation, heating, and cooling, thereby provide comprehensive insights into the material response under realistic conditions.

2.1.1. *Structural data*

Structural data describes the detailed chemical composition and bonding connectivity of each epoxy–hardener system. In our work, this data is represented at the molecular level using SMILES strings [33,34]. SMILES strings offer a standardized, linear notation that concisely encodes critical molecular features such as backbone modifications, ring structures, and side-chain polarity. This uniform representation enables us to systematically capture variations in chemical structure (e.g., differences in backbone length, ring substituents, or polarity) across the diverse formulations, which is essential for accurate modeling of the thermomechanical behavior.

2.1.2. *Temporal data*

Temporal data captures the time-dependent behavior of the polymers during the simulated thermomechanical cycle. Specifically, a set of key features such as time steps, temperature profiles, sample length, and moving-averaged stress is recorded to characterize the dynamic response of the material. These features are critical for understanding how the polymers evolve under varying thermal and mechanical conditions. Table 1 presents a summary of the temporal features and details both the experimental conditions and the corresponding outputs that reflect the material's recovery behavior.

2.2. *Epoxy and hardener types*

The selection of epoxy resins and diamine hardeners is essential for exploring the wide spectrum of thermomechanical behaviors in SMPs. Our dataset comprises both traditional commercial formulations and novel, custom-engineered variants, and captures a diverse range of chemical architectures and performance characteristics.

2.2.1. *Epoxy resins*

Diglycidyl ether-based epoxies generally offer robust mechanical properties and tunable shape-memory characteristics [6]. To broaden the chemical space, certain base epoxies were systematically modified by adjusting backbone length, side-chain polarity, and ring architecture, as guided by MD insights that show aromatic content, backbone rigidity, and side-chain substitutions strongly affect recovery stress [31, 32]. Table 2 summarizes the primary epoxy resins used in this study.

2.2.2. *Hardener*

Amine-based hardeners provide the reactive sites essential for forming permanent cross-links in thermoset networks, which in turn determine the network structure and mechanical performance. Table 3 lists the primary diamine hardeners in our dataset, each exhibits distinct structural features that influence key properties such as glass transition temperature, recovery stress, and overall thermomechanical behavior.

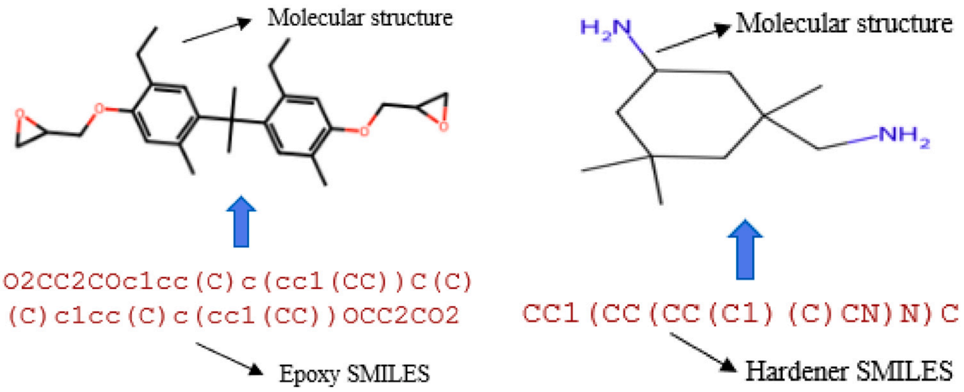

(a) (b)

Fig. 2. SMILES string to Molecular representation from composition DGEBA271-IPD. (**a**) Epoxy DGEBA271. (**b**) Hardener IPD.

Table 3
Diamine hardeners used in this study.

Hardener	Compound name	Description
IPD	Isophorone diamine	Commercial diamine balancing rigidity and processability.
APA	4-(4-Aminophenyl) Aniline	Aromatic diamine known to enhance recovery stress and thermal stability.
mPDA	m-Phenylenediamine	Aromatic diamine contributing to high cross-link density and thermal stability.
dMPDA	Modified m-Phenylenediamine	Custom derivative of mPDA designed for enhanced mechanical stability and adjustable glass transition temperature.
dDAP	Modified Diaminodiphenyl	Custom derivative of DAP, designed to optimize recovery stress.
autohardener	Computationally Designed Hardener	Generated diamine with novel structural motifs for enhanced thermomechanical performance.

2.3. SMILES strings

As described in Section 2.1.1, the molecular structures of epoxy resins and hardeners are encoded using SMILES strings, which offer a concise, linear representation of atoms, bonds, ring positions, and side-chain configurations. For example, in our work we used diglycidyl ether of bisphenol A (DGEBA) as an epoxy resin and isophorone diamine (IPD) as a hardener.

The SMILES string for DGEBA 271 (a variant of Diglycidyl Ether of Bisphenol A):

```
O2CC2COc1cc(C)c(cc1(CC))C(C)(C)c1cc(C)c(cc1(CC))
    OCC2CO2
```

SMILES string for IPD (a diamine hardener):

```
CC1(CC(CC(C1)(C)CN)N)C
```

2.4. SMILES strings to molecular representation

The cheminformatics library RDKit was used to convert the SMILES strings into detailed molecular representations. This conversion extracts comprehensive information about the atoms and bond features of each molecular structure. Fig. 2 illustrates the transformation from SMILES strings to molecular structures for both the epoxy resin and the hardener.

2.5. Molecular structures to graph representation

To effectively utilize the molecular structures of epoxy resins and hardeners in our proposed model, we transformed SMILES-based molecular representations into structured molecular graphs. A molecular graph $G = (V, E)$ is defined by a set of nodes V, where each node $v_i \in V$ represents an atom, and a set of edges E, where each edge $e_{ij} \in E$ represents a chemical bond between atoms v_i and v_j. Each node v_i is characterized by a detailed node feature vector, and each edge e_{ij} by a corresponding edge feature vector.

2.5.1. Node feature extraction

Node features capture essential chemical properties of individual atoms, providing vital contextual information for accurate molecular modeling. In our implementation, we employ RDKit to convert molecular SMILES representations into structured molecular graphs, where each atom constitutes a node in the graph. For each node, we construct a comprehensive feature vector by integrating multiple categorical atom properties, each encoded using one-hot encoding.

Specifically, each node feature vector includes the atom type, the number of heavy atom neighbors, and the formal charge. The type of atom is encoded from a predefined list of 43 chemically relevant elements, which includes common non-metal elements such as carbon (C), nitrogen (N), oxygen (O) and sulfur (S), as well as selected metals and metalloids including magnesium (Mg), sodium (Na), calcium (Ca), and iron (Fe). To robustly handle rare or unanticipated elements, we also include an “Unknown” category. Consequently, each atom type is represented by a 43-dimensional one-hot encoded vector. Additionally, the number of heavy atom neighbors, defined as the count of directly bonded non-hydrogen atoms, is encoded into six discrete categories (ranging from 0 to 4, plus an additional “MoreThanFour” category for atoms exceeding four neighbors). Similarly, formal charges are encoded into eight distinct categories, with extreme or rare charges grouped under a single “Extreme” category. Concatenating these categorical encodings results in a detailed and chemically meaningful node feature vector of dimension 57. Node feature vectors for all atoms in a molecule are aggregated into a node feature matrix X of shape $[N, 57]$, where N denotes the total number of nodes and forms a structured input for our graph-based model.

2.5.2. Edge index construction

Graph connectivity is captured by constructing an edge index that encodes bond relationships between atoms. For every bond identified in the molecule, indices of the two connected atoms are recorded. To explicitly represent undirected bonds, each bond contributes two directed edges: one from atom v_i to atom v_j, and another in the reverse direction. These index pairs are collected and converted into a tensor of shape $[2, E]$, where E is the total number of directed edges.

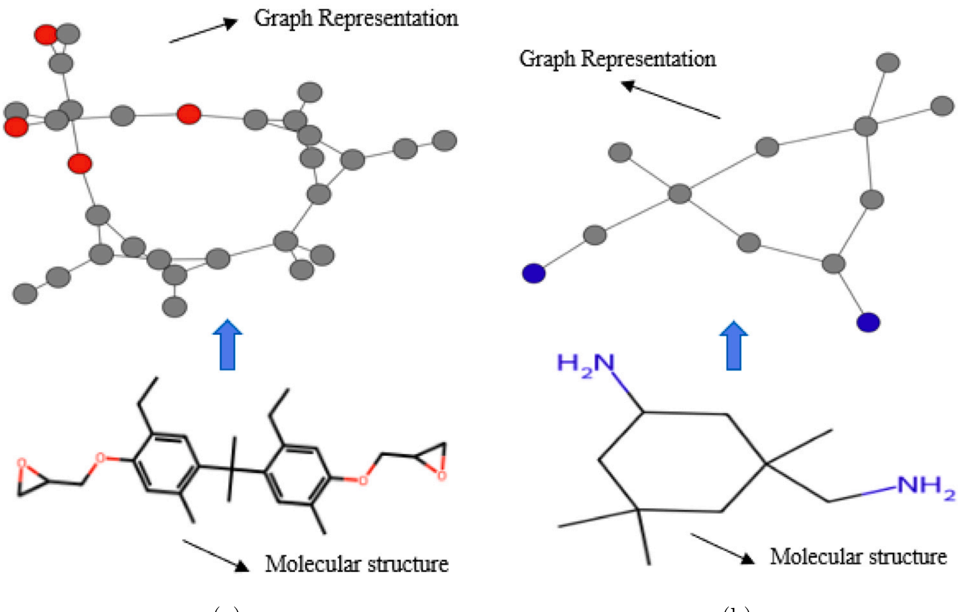

(a) (b)

Fig. 3. Transformation from molecular structure to graph representation for the composition `DGEBA271-IPD`. (**a**) Epoxy `DGEBA271`. (**b**) Hardener `IPD`.

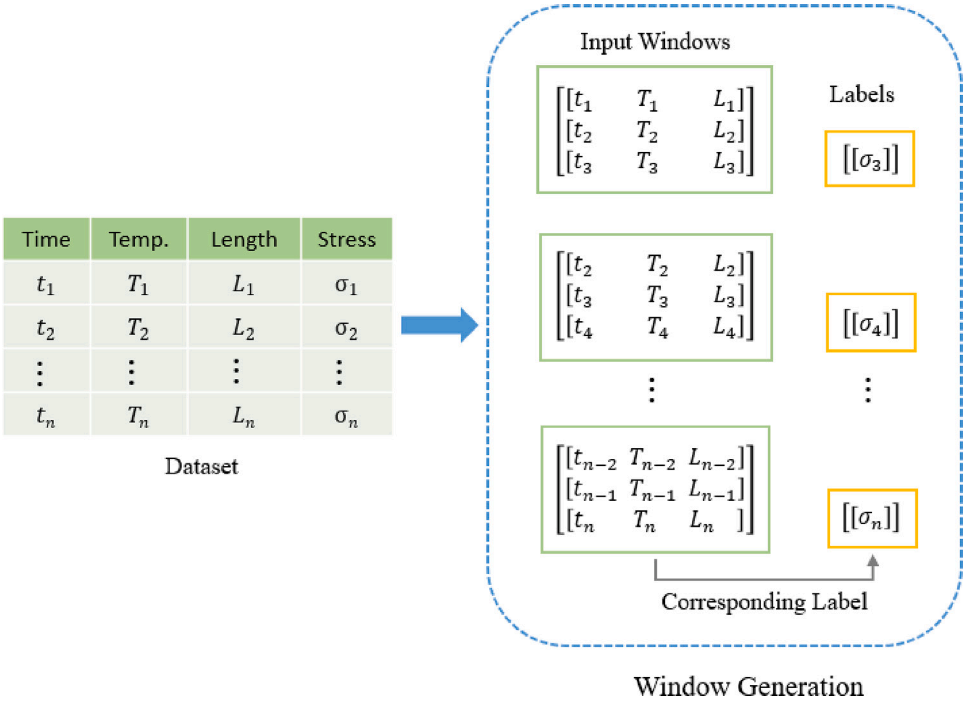

Time	Temp.	Length	Stress
t_1	T_1	L_1	σ_1
t_2	T_2	L_2	σ_2
⋮	⋮	⋮	⋮
t_n	T_n	L_n	σ_n

Fig. 4. An overview of window generation, where the input windows are the sequence of input features (time, temperature and length) and output features are the values of stress at the final time step of each corresponding input window.

2.5.3. Edge feature extraction

Edge features are computed to incorporate chemical bond characteristics into the graph representation. For each edge representing a chemical bond, a categorical one-hot encoding is performed based on its type (single, double, triple, or aromatic) which results a four-dimensional feature vector. Similar to the edge index, each edge feature vector is duplicated for both bond directions to maintain the undirected nature of chemical bonds. These edge feature vectors are then collated into a tensor with shape $[E, 4]$, where E corresponds to the total number of directed edges.

2.5.4. Graph construction

Having extracted node and edge features, the molecular graph is constructed by combining the node feature matrix X, the edge index tensor, and the edge feature matrix. Utilizing RDKit, SMILES strings are converted into molecular objects from which atom-level and bond-level information are obtained. The adjacency information provided by RDKit allows identification of connected atom pairs, which form the basis of the edge index tensor. This tensor is associated with the corresponding edge feature vectors derived previously.

Finally, the node feature matrix, edge connectivity tensor, and edge feature matrix are consolidated into a structured data object using

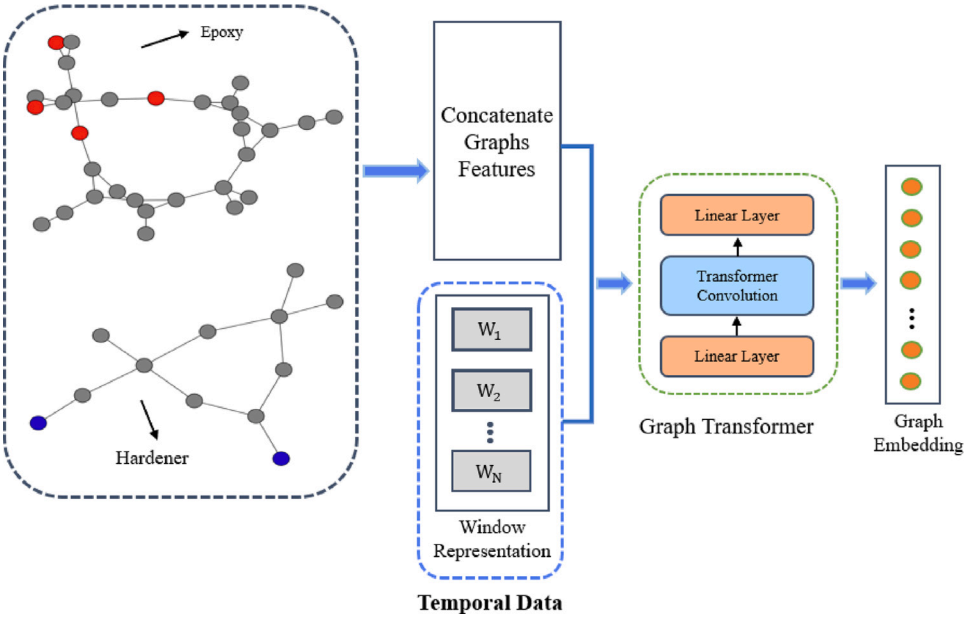

Fig. 5. An overview of generating graph embedding from the graph representations of epoxy resins and hardener. The method takes graph representations as input into the Graph Transformer model that gives the graph embedding from the combination of two molecular graph structures.

PyTorch Geometric. This unified graph representation encapsulates comprehensive molecular structure information, enabling effective integration into our proposed model. Fig. 3 provides a visual summary of the transformation from SMILES-based molecular representations to structured graph representations, and explicitly highlights the nodes (atoms) and edges (bonds) for representative epoxy resin and hardener molecules.

2.6. Temporal data: Sequence of windows

We have data from several epoxy–hardener systems, each of these systems has the input features: time, temperature and length and the output feature: recovery stress. To train the transformer model and our proposed model, we normalize the dataset using a z-score normalization which scales each of the variables into the dataset with a mean of 0 and a standard deviation 1. We use the normalization formula is follows:

$$z_i = \frac{x_i - \mu}{\sigma}, \tag{1}$$

where x_i and z_i are the original values and the normalized values respectively, μ and σ are the mean and standard deviation of the original data respectively.

We structure the dataset into sequence of windows where each window is comprised of n (we called it window size) number of consecutive time steps of input features and the output is the corresponding target value of each window at the final time step of that window. As depicted into Fig. 4, the input windows are consisted of 3 consecutive time steps of input features while the output is the target value at the third time step of that window. The number of consecutive time steps can be changed based on the experiment's requirements. In our experiments, we used the window size $n = 4$ for all the experiments.

2.7. Graph embedding generation

In our proposed method, as presented in Fig. 5, we generate the graph embedding from the graph representations of the SMILES of the epoxy and hardener molecules. To generate the graph embedding from the graph representations, we concatenate the graph representations of the SMILES of both molecules. This concatenated graph features along with the temporal data goes through a GNN to generate the graph embedding. To input the temporal data, we considered the sequence of windows from the time series data. Our goal was to generate different graph embedding at each time step of the time series data, we call it dynamic graph embedding. For our graph embedding generation we used Graph Transformer for the GNN. This is the first part of our proposed model where we generate the dynamic embedding, then this graph embedding along with the temporal data pass through another DL model to predict the final output. This proposed model is then trained in an end to end manner where the parameters in both the Graph Transformer and in the DL model are updated in the same training.

2.7.1. Graph transformer

In our Graph Transformer Networks [35], we use a fully connected layer to map the node features into a higher dimensional latent space. Then multiple Transformer convolutional layers with multi head self-attention were applied to capture complex interactions among nodes which effectively aggregate multi-hop neighborhood information and learns adaptive complex path. After these layers, we apply a global mean pooling to the resulting node features to form a graph embedding that combine all the node features into one overall graph representation. We apply a linear transformation in the final layer to fine tune the graph embedding. Additionally, to accommodate the temporal dynamics, we update the static graph features by concatenating them with the time-series data. This integration of time series data with the graph representation enable the model to generate the dynamic graph embeddings at each time step that captures both structural and temporal variations in our graph data. In our experiments, the Graph Transformer architecture consists of 4 Transformer convolutional layers, each with 4 attention heads. These layers are followed by a single-layer feedforward neural network without an activation function, which serves as a linear transformation to refine the final graph embedding.

2.8. End to end training with structural and temporal data

In our proposed method, we combine both the temporal data and dynamic graph embedding generated by the graph transformer and then use this as the input to the Time Series Transformer to predict the final output. For each time step, we append the graph embedding which

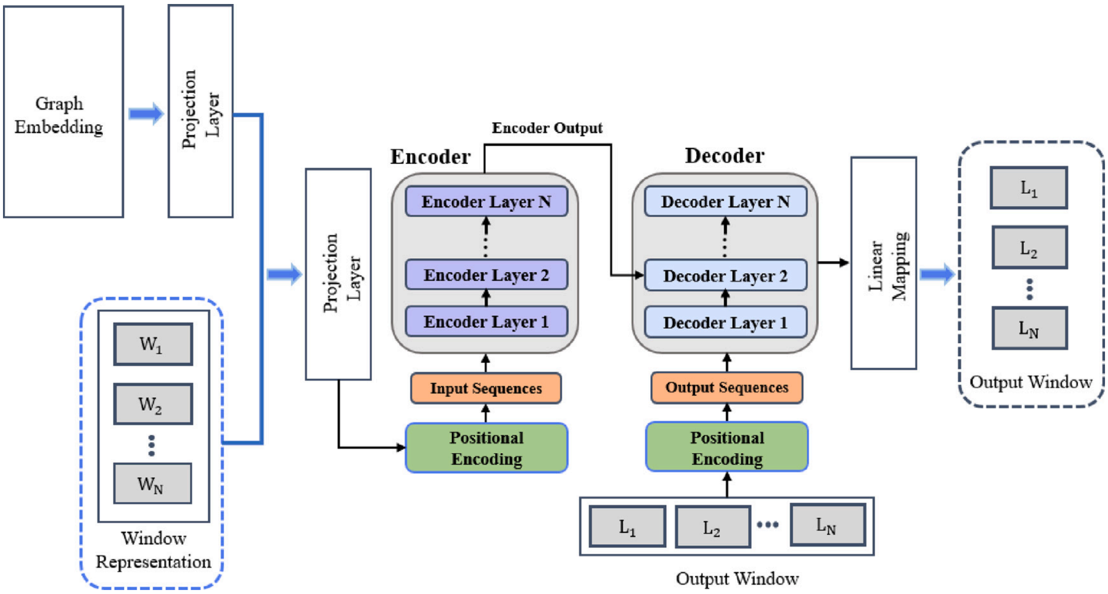

Fig. 6. An overview of the Time Series Transformer for predicting stress of the composition of epoxy resins and hardener. The graph embedding combined with the temporal data are the input to the Time Series Transformer.

has both structural and temporal context, to the corresponding time series features. This combination is then passed into the Time Series Transformer, which predicts the output at the final time step of each input window. The overall model is trained in an end-to-end manner, where both the Graph Transformer and the time series Transformer adjust their parameters together during training. An overview of the Time Series Transformer is presented in Fig. 6.

2.8.1. Time series transformer

The Time Series Transformer [30,36] processes the dynamic graph embeddings along with the time-series data using an encoder–decoder architecture with multi-head attention, demonstrated in Fig. 6. It can capture both short-term and long-range temporal dependencies in the input.

Each time-series window, along with its corresponding graph embedding, is projected into a higher-dimensional space. Then the positional encodings are added to maintain temporal order. The encoder consists of multiple layers of multi-head self-attention and position-wise feed-forward networks transform the input window into a rich contextual representation. The decoder uses additional attention mechanisms to focus on relevant parts of the encoded input while integrating dynamic graph embeddings for accurate prediction. Residual connections and normalization are applied throughout to ensure stable training. In the final step, a fully connected output layer generates the predicted stress value at the last time step of each input window. In our experiments, the Time Series Transformer architecture utilized a window size of 4 for the time-series data. Specifically, the architecture consists of 4 encoder layers and 4 decoder layers, each with 4 attention heads and a model dimension of 256. The model was trained for 30 epochs with a batch size of 8, using the Adam optimizer with a learning rate of 0.0001, weight decay of 0.0001, and a dropout rate of 0.1 for regularization.

2.9. Deep learning models for temporal data

We evaluated several DL models that utilize temporal data alone to predict the recovery stress of diamine-hardened epoxy-based thermoset SMPs. The models include feed-forward neural networks (FNN) [28,37], convolutional neural networks (CNN) [38–41], Long Short-Term Memory networks (LSTM) [42,43], convolutional LSTM (ConvLSTM) [44], and convolutional bidirectional LSTM (ConvBiLSTM) [45].

The FNN architecture employs a multi-headed structure that independently processes each temporal feature through embedding layers followed by fully connected layers, dropout regularization, and final concatenation. This approach effectively captures non-linear relationships among features without explicitly modeling sequential dependencies. CNN architectures leverage convolutional layers followed by pooling operations and dense layers to extract local temporal patterns and structural features inherent in the data. These networks are particularly adept at identifying short-range dependencies and intricate temporal patterns in the SMP dataset. The LSTM model, known for its capability to capture long-range temporal dependencies, employs stacked recurrent layers with gating mechanisms (input, forget, and output gates) that effectively manage information flow. This design mitigates the vanishing gradient problem commonly encountered with traditional recurrent neural networks.

Hybrid convolutional-recurrent models such as ConvLSTM and ConvBiLSTM integrate convolutional operations directly into LSTM architectures. ConvLSTM utilizes spatial convolutional structures within recurrent layers to simultaneously learn spatially local features and sequential temporal dependencies. ConvBiLSTM extends this approach by processing sequences in both forward and backward directions, thus capturing contextual information from past and future time steps, enhancing overall prediction performance.

All models were trained using the Adam optimizer, incorporating appropriate regularization techniques and hyperparameter tuning to ensure robust and optimal predictive accuracy.

3. Experiments and results

3.1. Evaluation metrics

We used two performance evaluation matrices to evaluate the performance of the models: Root Mean Squared Error (RMSE) and Pearson Correlation Coefficient (PCC) [46]. RMSE measures the error between the predicted and actual values by taking the square root of the mean of squared errors. PCC, on the other hand, evaluates the linear association between predictions and ground truth values, where a value closer to 1 signifies a stronger positive correlation. The RMSE is defined as follows:

$$\mathrm{RMSE} = \sqrt{\frac{1}{N}\sum_{i=1}^{N}(y_i - \hat{y}_i)^2}, \tag{2}$$

Table 4

Performance metrics (RMSE and PCC) of FNN, CNN, LSTM, ConvLSTM, ConvBiLSTM, and proposed model on datasets varying the epoxy only in epoxy-hardened compositions.

Dataset	FNN		CNN [41]		LSTM		ConvLSTM		ConvBiLSTM [45]		Proposed model	
	RMSE ↓	PCC ↑	RMSE ↓	PCC ↑	RMSE ↓	PCC ↑	RMSE ↓	PCC ↑	RMSE ↓	PCC ↑	RMSE ↓	PCC ↑
`autoDGEBA326-IPD`	33.6682	0.9216	28.7264	0.8383	28.6062	0.8700	27.3926	0.8536	23.8467	0.8828	**1.3920**	**0.9996**
`autoEpoxy2_590-IPD`	21.5371	0.9435	22.80	0.8544	25.3078	0.8303	21.4029	0.8872	22.2296	0.8755	**0.6576**	**0.9999**
`autoEpoxy2_545-IPD`	28.9431	0.8991	25.7778	0.8076	24.4269	0.8272	25.5264	0.8098	23.2852	0.8312	**0.3514**	**1.0000**
`autoEpoxy2256-IPD`	36.1205	0.9431	35.9513	0.8754	38.8733	0.8298	36.2168	0.9124	35.1469	0.8555	**5.5519**	**0.9967**
`autoEpoxy2348-IPD`	54.3062	0.9329	48.4626	0.8187	51.8248	0.7993	46.9010	0.8613	44.1809	0.8495	**7.4385**	**0.9959**
`autoEpoxy2394-IPD`	49.0315	0.9131	42.4680	0.8162	45.0538	0.8142	41.6072	0.8242	39.0672	0.8330	**4.9127**	**0.9984**
`autoEpoxy3084-IPD`	42.7393	0.9353	41.4884	0.8259	43.4070	0.8089	40.8969	0.8668	38.5956	0.8479	**4.5118**	**0.9978**
`DGEBF-IPD`	16.0836	0.9079	25.8590	0.8825	23.5002	0.8501	32.5061	0.8191	32.9510	0.8363	**0.1895**	**1.0000**

Table 5

Performance metrics (RMSE and PCC) of FNN, CNN, LSTM, ConvLSTM, ConvBiLSTM, and proposed model on datasets varying the epoxy and hardener both in epoxy-hardened compositions.

Dataset	FNN		CNN [41]		LSTM		ConvLSTM		ConvBiLSTM [45]		Proposed model	
	RMSE ↓	PCC ↑	RMSE ↓	PCC ↑	RMSE ↓	PCC ↑	RMSE ↓	PCC ↑	RMSE ↓	PCC ↑	RMSE ↓	PCC ↑
`autoEpoxy2_590-APA`	41.9193	0.9437	38.4127	0.8471	44.6906	0.8073	39.4081	0.8625	36.1374	0.8539	**5.9505**	**0.9971**
`autoEpoxy2_409-APA`	60.2272	0.9238	57.8208	0.8790	56.0781	0.8773	56.3111	0.9009	53.4950	0.8841	**9.6100**	**0.9927**
`autoEpoxy2_592-APA`	32.7297	0.9401	32.3868	0.8189	35.6418	0.8019	30.4658	0.8449	28.2723	0.8619	**2.2924**	**0.9993**
`DGEBA-Autohardener70`	31.0650	0.9534	28.3956	0.8626	33.7135	0.8328	26.7087	0.8883	28.6038	0.8558	**3.9013**	**0.9983**
`DGEBA-Autohardener40`	22.5000	0.9044	24.8558	0.8371	25.9302	0.8255	24.1105	0.8425	28.2789	0.8203	**0.4988**	**0.9999**
`DGEBA-dDAP_Base134`	25.9266	0.9354	27.1780	0.8314	29.6270	0.8091	26.0556	0.8543	23.6386	0.8760	**1.6061**	**0.9996**
`DGEBA-dMPDA_Base117`	64.7011	0.8653	61.2631	0.6702	60.92	0.7019	53.8625	0.7303	49.1432	0.8014	**7.6781**	**0.9959**
`DGEBA-dMPDA_Base227`	37.5867	0.9204	39.0495	0.7516	40.4150	0.7624	37.8014	0.7949	30.4593	0.8565	**3.3884**	**0.9985**

where y_i is the actual value, $\hat{y}_i$ is the predicted value, and N is the total number of data points.

The PCC is computed as follows:

$$\mathrm{PCC} = \frac{\sum_{i=1}^{N} (y_i - \bar{y})(\hat{y}_i - \bar{\hat{y}})}{\sqrt{\sum_{i=1}^{N} (y_i - \bar{y})^2 \sum_{i=1}^{N} (\hat{y}_i - \bar{\hat{y}})^2}}, \tag{3}$$

where y_i and $\hat{y}_i$ are the actual and predicted values, respectively, and $\bar{y}$ and $\bar{\hat{y}}$ are their mean values.

3.2. Results and discussion

After preprocessing the dataset, we evaluated multiple DL models, including FNN, CNN, LSTM, ConvLSTM, ConvBiLSTM, and our proposed GNN based DL model for predicting the recovery stress in diamine-hardened epoxy-based thermoset SMPs. Initially, all models were trained exclusively on the `autoDGEBA271-IPD` dataset, partitioned into an 70:20:10 ratio (70% training, 20% validating and 10% testing). Subsequently, we assessed the trained models' predictive performance on multiple completely unseen epoxy–hardener formulations to evaluate their generalization capability.

To ensure consistency, all unseen test datasets were normalized using the mean and standard deviation derived exclusively from the `autoDGEBA271-IPD` training dataset. The predictive performance metrics (RMSE and PCC) for each model across all datasets are summarized in two different tables separately: Table 4 presents results for datasets varying only the epoxy component (with IPD hardener constant), while Table 5 shows results for datasets where both epoxy and hardener components differ from the training set.

The results in Tables 4 and 5 clearly demonstrate that our proposed model significantly outperformed all baseline temporal-only models: FNN, CNN, LSTM, ConvLSTM, and ConvBiLSTM across every dataset tested. For example, in the `autoDGEBA326-IPD` dataset (epoxy variant) in Table 4, our model achieved an RMSE of 1.3920 and a PCC of 0.9996, which significantly outperforms the second best temporal-only model (ConvBiLSTM) and attained an RMSE of 23.8467 and a PCC of 0.8828. Similarly, in a more challenging scenario where both epoxy and hardener components differ (`autoEpoxy2_590-APA`) in Table 5, our model maintained outstanding predictive accuracy (RMSE = 5.9505, PCC = 0.9971), and significantly outperforms all other models.

Among purely temporal models, the ConvBiLSTM consistently delivered superior predictive performance relative to simpler models like FNN, CNN, and LSTM, which reflects the advantages of simultaneously capturing local spatial patterns and bidirectional temporal dependencies in the data. Specifically, ConvBiLSTM exhibited lower RMSE and higher PCC values compared to other temporal-only models in almost all tested datasets. For example, on the `autoEpoxy2_545-IPD` dataset in Table 4, ConvBiLSTM yielded an RMSE of 23.2852, compared to the significantly higher RMSE of 28.9431 for FNN and 25.5264 for ConvLSTM. This observation underscores the effectiveness of hybrid convolutional-recurrent architectures in extracting intricate temporal patterns from sequential polymer data.

Notably, simple sequential models such as LSTM showed inconsistency in data sets and displayed relatively higher prediction errors and weaker correlations compared to convolutional architectures (CNN, ConvLSTM, ConvBiLSTM). This inconsistency highlights the limitations of sequential-only methods when attempting to accurately model complex thermomechanical responses based solely on temporal information. Additionally, the FNN, despite its computational simplicity, generally showed moderate performance across datasets. However, its predictions lacked stability and precision compared to the more advanced architectures.

The significant improvement demonstrated by our proposed model can be attributed directly to its unique capability of integrating molecular structural features alongside temporal data. Specifically, by utilizing dynamic molecular graph embeddings generated through a Graph Transformer and subsequently integrating these embeddings with temporal context using a Time Series Transformer, the model effectively captures structural variations between different epoxy and hardener formulations. This capability allowed it to accurately generalize across unseen formulations, substantially enhancing its predictive robustness compared to temporal-only methods.

To visually demonstrate this superior predictive performance, Fig. 7(f) closely align with the ground truth, and consistently maintains lower errors across the entire temporal range. In contrast, the FNN (Fig. 7(a)), CNN (Fig. 7(b)), LSTM (Fig. 7(c)), ConvLSTM (Fig. 7(d)), and ConvBiLSTM (Fig. 7(e)) all exhibit significantly higher prediction errors, which shows their limitations in capturing the complex interplay between structural variations and temporal dynamics inherent in SMPs.

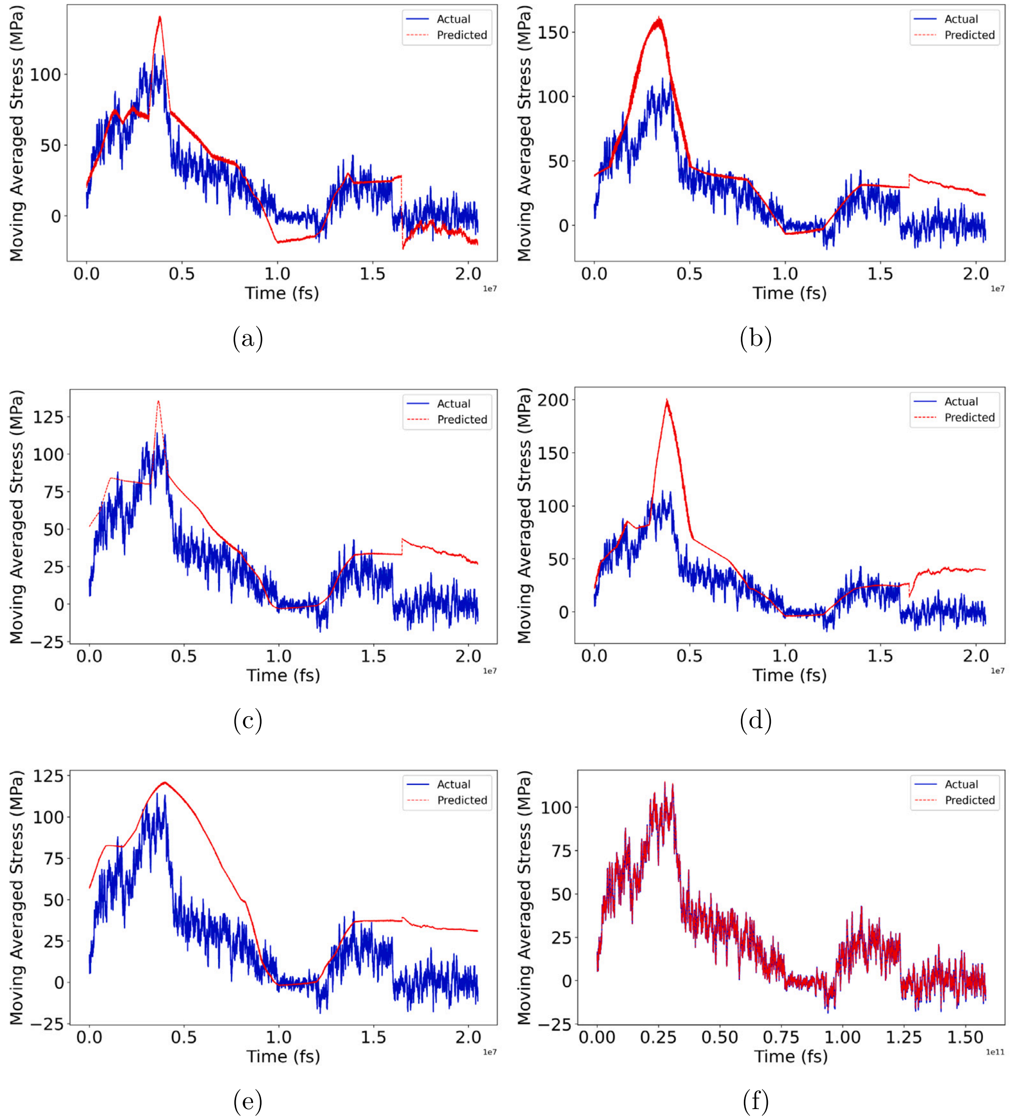

(a) (b) (c) (d) (e) (f)

Fig. 7. Performance of DL models and our proposed model in predicting the moving averaged stress on dataset `DGEBF-IPD`: (a) FNN, (b) CNN, (c) LSTM, (d) ConvLSTM, (e) ConvBiLSTM and (f) Our proposed model.

Our proposed model employs a Graph Transformer to encode structural features of epoxy–hardener molecules, and captures the comprehensive atomic and bonding information. By integrating these dynamically updated molecular graph embeddings with temporal data using a Time Series Transformer, the model effectively accounts for structural variations and temporal dependencies simultaneously. This combined modeling strategy significantly enhances predictive accuracy and enables a more robust and precise characterization of stress recovery behavior compared to methods relying solely on temporal features. Consequently, the approach demonstrates superior generalization capability and improved prediction robustness across unseen epoxy–hardener compositions.

4. Conclusion and future work

In this study, we proposed and evaluated a novel deep learning (DL) framework that integrates Graph Neural Networks (GNNs) with Time Series Transformers to predict the moving-averaged recovery stress—a key thermomechanical property—of diamine-hardened epoxy-based thermoset shape memory polymers (SMPs). By combining molecular graph representations derived from SMILES strings with temporal data such as time, temperature, and length, our model captures both chemical structure and dynamic material behavior. This joint structural–temporal representation enabled our model to outperform conventional temporal-only baselines (e.g., FNN, CNN, LSTM, ConvLSTM, ConvBiLSTM) in terms of RMSE and PCC.

Our findings demonstrate the critical role of integrating molecular structure with temporal experimental data for accurate moving-averaged recovery stress prediction. Models that relied solely on time-series inputs showed reduced predictive power and poor generalization across varying epoxy–hardener systems. In contrast, our proposed framework, which dynamically combines graph-based molecular embeddings with sequential experimental features, achieved superior performance in both RMSE and PCC. This fusion of structural and temporal domains not only improved accuracy but also significantly reduces the need for costly and repetitive experimental testing, offering a more efficient route for screening and designing high-performance SMP formulations.

In our future work, we plan to improve the predictive capability and practical applicability of our framework along several directions. First, we will address the timescale gap between MD simulations (femtoseconds to microseconds) and real-world stress recovery (seconds to minutes) by employing multiscale modeling approaches.

These include coupling MD-based outputs with coarse-grained viscoelastic models and calibrating predictions using experimental TMA data through transfer learning and ranking-based validation. Second, to better represent chemical reactivity, we will incorporate quantum-chemical descriptors—such as HOMO-LUMO gaps, partial charges, activation energies, and reaction barriers—computed using methods like density functional theory (DFT). These features will be embedded into our graph representation to more accurately capture curing dynamics and crosslink formation [47,48]. Third, we aim to extend our framework to handle multi-component systems, which are common in industrial thermoset formulations, by constructing composite molecular graphs and adapting attention mechanisms to capture complex intermolecular interactions. Finally, a key long-term goal is to integrate and validate the model with available experimental datasets, enhancing robustness and enabling real-world deployment for data-driven polymer discovery and optimization.

CRediT authorship contribution statement

Khan Raqib Mahmud: Writing – original draft, Visualization, Software, Methodology, Investigation, Formal analysis, Data curation, Conceptualization. **Lingxiao Wang:** Writing – review & editing, Validation, Supervision, Resources, Project administration, Methodology, Funding acquisition, Data curation, Conceptualization. **Jinyuan Chen:** Writing – review & editing, Validation, Data curation, Conceptualization. **Sunzid Hassan:** Writing – review & editing.

Declaration of competing interest

The authors declare the following financial interests/personal relationships which may be considered as potential competing interests: Lingxiao Wang reports was provided by State of Louisiana Board of Regents. If there are other authors, they declare that they have no known competing financial interests or personal relationships that could have appeared to influence the work reported in this paper.

Acknowledgments

The authors gratefully appreciate the assistance of Dr. Andrew Peters, Associate Professor, Center for Biomedical Engineering and Rehabilitation Sciences, Chemical Engineering, Institute for Micromanufacturing, Louisiana Tech University, Ruston, LA and Diego Segura Ibarra, Department of Electrical Engineering, Louisiana Tech University, Ruston, LA for their help with the datasets.

Data availability

Data will be made available on request.

References

[1] W. Huang, Z. Ding, C. Wang, J. Wei, Y. Zhao, H. Purnawali, Shape memory materials, Mater. Today 13 (7) (2010) 54–61.

[2] H. Meng, G. Li, A review of stimuli-responsive shape memory polymer composites, Polymer 54 (9) (2013) 2199–2221.

[3] W. Sokolowski, A. Metcalfe, S. Hayashi, L. Yahia, J. Raymond, Medical applications of shape memory polymers, Biomed. Mater. 2 (1) (2007) S23–S27.

[4] Y. Liu, H. Du, L. Liu, J. Leng, Shape memory polymers and their composites in aerospace applications: a review, Smart Mater. Struct. 23 (2) (2014).

[5] S. Thakur, Shape memory polymers for smart textile applications, Text. Adv. Appl. 10 (2017) S323–S338.

[6] C. Yan, X. Feng, C. Wick, A. Peters, G. Li, Machine learning assisted discovery of new thermoset shape memory polymers based on a small training dataset, Polymer 214 (2021) 123351.

[7] J. Choi, H. Kang, J.H. Lee, S.H. Kwon, S.G. Lee, Predicting the properties of high-performance epoxy resin by machine learning using molecular dynamics simulations, Nanomaterials 12 (14) (2022).

[8] C. Yin, H. Zeng, J. Gu, Z. Xie, H. Sun, Modeling the thermomechanical behaviors of particle reinforced shape memory polymer composites, Appl. Phys. A 125 (6) (2019) 1–10, http://dx.doi.org/10.1007/S00339-019-2672-Z.

[9] W. Zhao, L. Liu, J. Leng, Y. Liu, Thermo-mechanical behavior prediction of particulate reinforced shape memory polymer composite, Compos. Part B-Eng. 179 (2019) 107455, http://dx.doi.org/10.1016/J.COMPOSITESB.2019.107455.

[10] S. Pal, K. Dansuk, A. Giuntoli, T.W. Sirk, S. Keten, Predicting the effect of hardener composition on the mechanical and fracture properties of epoxy resins using molecular modeling, Macromolecules 56 (2023) 4447–4456.

[11] R. Dutta, D. Renshaw, C. Chen, D. Liang, Machine learning based approach for shape memory polymer behavioural characterization, Array 7 (2020) 100036, http://dx.doi.org/10.1016/j.array.2020.100036.

[12] M. Heuchel, J. Cui, K. Kratz, H. Kosmella, A. Lendlein, Relaxation based modeling of tunable shape recovery kinetics observed under isothermal conditions for amorphous shape-memory polymers, Polymer 51 (26) (2010) 6212–6218.

[13] H. Lu, W.M. Huang, On the origin of the Vogel–Fulcher–Tammann law in the thermo-responsive shape memory effect of amorphous polymers, Smart Mater. Struct. 22 (10) (2013) 105021.

[14] M. Siwakoti, R.W. Mailen, Coupled electro-thermo-mechanical modeling of shape memory polymers, in: Smart Materials, Adaptive Structures and Intelligent Systems, vol. ASME 2019 Conference on Smart Materials, Adaptive Structures and Intelligent Systems, 2019, V001T02A011, http://dx.doi.org/10.1115/SMASIS2019-5693.

[15] K. Guo, Z. Yang, C.-H. Yu, M.J. Buehler, Artificial intelligence and machine learning in design of mechanical materials, Mater. Horiz. 8 (2021) 1153–1172.

[16] J. Wei, X. Chu, X. Sun, K. Xu, H. Deng, J. Chen, Z. Wei, M. Lei, Machine learning in materials science, InfoMat 1 (3) (2019) 338–358.

[17] J.-W. Lee, W.B. Park, B. Do Lee, S. Kim, N.H. Goo, K.-S. Sohn, Dirty engineering data-driven inverse prediction machine learning model, Sci. Rep. 10 (1) (2020) 20443.

[18] S. Wu, Y. Kondo, M.-a. Kakimoto, B. Yang, H. Yamada, I. Kuwajima, G. Lambard, K. Hongo, Y. Xu, J. Shiomi, et al., Machine-learning-assisted discovery of polymers with high thermal conductivity using a molecular design algorithm, Npj Comput. Mater. 5 (1) (2019) 66.

[19] A. Mannodi-Kanakkithodi, G. Pilania, T.D. Huan, T. Lookman, R. Ramprasad, Machine learning strategy for accelerated design of polymer dielectrics, Sci. Rep. 6 (1) (2016) 20952.

[20] C. Yan, G. Li, Machine learning framework for polymer discovery, Encycl. Mater.: Plast. Polym. 1 (2022) 267.

[21] L.A. Miccio, G.A. Schwartz, From chemical structure to quantitative polymer properties prediction through convolutional neural networks, Polymer 193 (2020) 122341.

[22] L. Tao, G. Chen, Y. Li, Machine learning discovery of high-temperature polymers, Patterns 2 (4) (2021) 100225.

[23] C. Yan, X. Feng, G. Li, From drug molecules to thermoset shape memory polymers: A machine learning approach, ACS Appl. Mater. Interfaces 13 (50) (2021) 60181–60194.

[24] K. Wang, W. Sun, A multiscale multi-permeability poroplasticity model linked by recursive homogenizations and deep learning, Comput. Methods Appl. Mech. Engrg. 334 (2018) 337–380.

[25] A.M. Tartakovsky, C.O. Marrero, P. Perdikaris, G.D. Tartakovsky, D. Barajas-Solano, Physics-informed deep neural networks for learning parameters and constitutive relationships in subsurface flow problems, Water Resour. Res. 56 (5) (2020) e2019WR026731.

[26] T. Kirchdoerfer, M. Ortiz, Data-driven computational mechanics, Comput. Methods Appl. Mech. Engrg. 304 (2016) 81–101.

[27] R. Ibanez, E. Abisset-Chavanne, J.V. Aguado, D. Gonzalez, E. Cueto, F. Chinesta, A manifold learning approach to data-driven computational elasticity and inelasticity, Arch. Comput. Methods Eng. 25 (1) (2018) 47–57, http://dx.doi.org/10.1007/s11831-016-9197-9.

[28] D.S. Ibarra, J. Mathews, F. Li, H. Lu, G. Li, J. Chen, Deep learning for predicting the thermomechanical behavior of shape memory polymers, Polymer 261 (2022) 125395, http://dx.doi.org/10.1016/j.polymer.2022.125395.

[29] Y. Shi, Z. Huang, S. Feng, H. Zhong, W. Wang, Y. Sun, Masked label prediction: Unified message passing model for semi-supervised classification, 2021, arXiv:2009.03509.

[30] N. Wu, B. Green, X. Ben, S. O'Banion, Deep transformer models for time series forecasting: The influenza prevalence case, 2020, arXiv:2001.08317.

[31] A. Shafe, C.D. Wick, A.J. Peters, X. Liu, G. Li, Effect of atomistic fingerprints on thermomechanical properties of epoxy-diamine thermoset shape memory polymers, Polymer 242 (2022) 124577.

[32] A. Shafe, P. Nourian, X. Liu, G. Li, C.D. Wick, A.J. Peters, Identification and design of better diamine-hardened epoxy-based thermoset shape memory polymers: Simulation and machine learning, Macromolecules 57 (21) (2024) 9933–9942.

[33] D. Weininger, SMILES, a chemical language and information system. 1. Introduction to methodology and encoding rules, J. Chem. Inf. Comput. Sci. 28 (1988) 31–36.

[34] D. Weininger, A. Weininger, J.L. Weininger, SMILES. 2. Algorithm for generation of unique SMILES notation, J. Chem. Inf. Comput. Sci. 29 (1989) 97–101.

[35] S. Yun, M. Jeong, R. Kim, J. Kang, H.J. Kim, Graph transformer networks, in: H. Wallach, H. Larochelle, A. Beygelzimer, F. d'Alché Buc, E. Fox, R. Garnett (Eds.), Advances in Neural Information Processing Systems, Vol. 32, Curran Associates, Inc., 2019.

[36] A. Vaswani, N. Shazeer, N. Parmar, J. Uszkoreit, L. Jones, A.N. Gomez, L.u. Kaiser, I. Polosukhin, Attention is all you need, in: I. Guyon, U.V. Luxburg, S. Bengio, H. Wallach, R. Fergus, S. Vishwanathan, R. Garnett (Eds.), Advances in Neural Information Processing Systems, Vol. 30, Curran Associates, Inc., 2017.

[37] M. Deprez, E.C. Robinson, Chapter 10 - Fully connected neural networks, in: M. Deprez, E.C. Robinson (Eds.), Machine Learning for Biomedical Applications, Academic Press, 2024, pp. 213–231.

[38] Z. Li, F. Liu, W. Yang, S. Peng, J. Zhou, A survey of convolutional neural networks: Analysis, applications, and prospects, IEEE Trans. Neural Netw. Learn. Syst. 33 (12) (2022) 6999–7019.

[39] J. Gu, Z. Wang, J. Kuen, L. Ma, A. Shahroudy, B. Shuai, T. Liu, X. Wang, G. Wang, J. Cai, T. Chen, Recent advances in convolutional neural networks, Pattern Recognit. 77 (2018) 354–377.

[40] A. Ayodeji, Z. Wang, W. Wang, W. Qin, C. Yang, S. Xu, X. Liu, Causal augmented ConvNet: A temporal memory dilated convolution model for long-sequence time series prediction, ISA Trans. 123 (2022) 200–217.

[41] A. Borovykh, S. Bohte, C.W. Oosterlee, Conditional time series forecasting with convolutional neural networks, 2017, arXiv preprint arXiv:1703.04691.

[42] P. Lara-Benítez, M. Carranza-García, J.C. Riquelme, An experimental review on deep learning architectures for time series forecasting, Int. J. Neural Syst. 31 (03) (2021) 2130001.

[43] S. Hochreiter, J. Schmidhuber, Long short-term memory, Neural Comput. 9 (8) (1997) 1735–1780.

[44] L. Jiao, W. Zheng, Multi-step traffic flow prediction method based on the Conv1D + LSTM, in: 2020 Eighth International Conference on Advanced Cloud and Big Data, CBD, 2020, pp. 113–118, http://dx.doi.org/10.1109/CBD51900.2020.00029.

[45] X. Shi, Z. Chen, H. Wang, D.-Y. Yeung, W. kin Wong, W. chun Woo, Convolutional LSTM network: A machine learning approach for precipitation nowcasting, 2015, arXiv:1506.04214.

[46] V. Plevris, G. Solorzano, N. Bakas, M.B. Seghier, Investigation of performance metrics in regression analysis and machine learning-based prediction models, in: Proceedings of ECCOMAS 2022, 2022.

[47] T. Okabe, T. Takehara, K. Inose, N. Hirano, M. Nishikawa, T. Uehara, Curing reaction of epoxy resin composed of mixed base resin and curing agent: Experiments and molecular simulation, Polymer 54 (17) (2013) 4660–4668, http://dx.doi.org/10.1016/j.polymer.2013.06.026.

[48] Y. Xi, H. Fukuzawa, S. Fukunaga, G. Kikugawa, Y. Zhao, Y. Kawagoe, T. Okabe, N. Kishimoto, Development of cat-GRRM/MC/MD method for the simulation of cross-linked network structure formation with molecular autocatalysis, Mol. Catal. 552 (2024) 113680, http://dx.doi.org/10.1016/j.mcat.2023.113680.